JOURNAL OF BACTERIOLOGY, Apr. 2004, p. 2240–2252 Vol. 186, No. 8
0021-9193/04/$08.00+0 DOI: 10.1128/JB.186.8.2240–2252.2004

Transcriptional Organization and Posttranscriptional Regulation of the *Bacillus subtilis* Branched-Chain Amino Acid Biosynthesis Genes

Ulrike Mäder,† Susanne Hennig,‡ Michael Hecker, and Georg Homuth*

Institut für Mikrobiologie und Molekularbiologie, Ernst-Moritz-Arndt-Universität Greifswald, D-17487 Greifswald, Germany

Received 22 September 2003/Accepted 23 December 2003

In *Bacillus subtilis*, the genes of the branched-chain amino acids biosynthetic pathway are organized in three genetic loci: the *ilvBHC-leuABCD* (*ilv-leu*) operon, *ilvA*, and *ilvD*. These genes, as well as *ybgE*, encoding a branched-chain amino acid aminotransferase, were recently demonstrated to represent direct targets of the global transcriptional regulator CodY. In the present study, the transcriptional organization and posttranscriptional regulation of these genes were analyzed. Whereas *ybgE* and *ilvD* are transcribed monocistronically, the *ilvA* gene forms a bicistronic operon with the downstream located *ypmP* gene, encoding a protein of unknown function. The *ypmP* gene is also directly preceded by a promoter sharing the regulatory pattern of the *ilvA* promoter. The *ilv-leu* operon revealed complex posttranscriptional regulation: three mRNA species of 8.5, 5.8, and 1.2 kb were detected. Among them, the 8.5-kb full-length primary transcript exhibits the shortest half-life (1.2 min). Endoribonucleolytic cleavage of this transcript generates the 5.8-kb mRNA, which lacks the coding sequences of the first two genes of the operon and is predicted to carry a stem-loop structure at its 5′ end. This processing product has a significantly longer half-life (3 min) than the full-length precursor. The most stable transcript (half-life, 7.6 min) is the 1.2-kb mRNA generated by the processing event and exonucleolytic degradation of the large transcripts or partial transcriptional termination. This mRNA, which encompasses exclusively the *ilvC* coding sequence, is predicted to carry a further stable stem-loop structure at its 3′ end. The very different steady-state amounts of mRNA resulting from their different stabilities are also reflected at the protein level: proteome studies revealed that the cellular amount of IlvC protein is 10-fold greater than that of the other proteins encoded by the *ilv-leu* operon. Therefore, differential segmental stability resulting from mRNA processing ensures the fine-tuning of the expression of the individual genes of the operon.

In *Bacillus subtilis*, three genetic loci are involved in the biosynthesis of branched-chain amino acids: the *ilvBHC-leuABCD* (*ilv-leu*) operon including genes encoding acetolactate synthase (*ilvBH*), ketol-acid reductoisomerase (*ilvC*), 2-isopropylmalate synthase (*leuA*), 3-isopropylmalate dehydrogenase (*leuB*), and 3-isopropylmalate dehydratase (*leuCD*); the *ilvA* gene encoding threonine dehydratase; and the *ilvD* gene encoding dihydroxy-acid dehydratase. These enzymes catalyze the formation of the α-keto acid precursors of isoleucine, valine, and leucine. In the final biosynthetic reaction, the α-keto acids are converted to the respective amino acids by transamination. Previous studies demonstrated that the *ilv-leu* operon is regulated in response to leucine availability by the T-box transcription antitermination system (14, 30). The common T-box-dependent regulatory mechanism of the biosynthetic *ilv-leu* operon and the aminoacyl-tRNA synthetase genes (15, 34) would be predicted to result in the coregulation of these genes. However, our global study of *B. subtilis* gene expression in response to amino acid availability (29) revealed that the *ilv-leu* operon was downregulated in the presence of Casamino Acids (CAA), whereas expression of the aminoacyl-tRNA synthetase genes was not affected under the same conditions. Furthermore, we found that all three transcriptional units involved in the biosynthesis of branched-chain amino acids, as well as the *ybgE* gene encoding a branched-chain amino acid aminotransferase, exhibited reduced expression levels in the presence of CAA. Although the genes for branched-chain amino acid biosynthesis share this common regulatory pattern, a genome-wide search revealed no T-box leader sequences upstream of *ilvA*, *ilvD*, and *ybgE* (6). Therefore, we were interested in identifying the regulatory mechanism responsible for the common regulation of the genes involved in branched-chain amino acid biosynthesis. Since the CodY repressor was known to mediate amino acid repression of several *B. subtilis* genes, we supposed that CodY may function as the common regulator of these genes. Experiments which were carried out to test whether the *ilv-leu* operon and the *ilvA*, *ilvD*, and *ybgE* genes are under the control of CodY verified this hypothesis. In the meantime, Molle et al. (33) reported on the identification of new CodY regulated genes, and the genes for branched-chain amino acid biosynthesis, including *ybgE*, were among these newly identified direct CodY targets.

Many early-stationary-phase genes of *B. subtilis* are repressed by the global regulator CodY. Ratnayake-Lecamwasam et al. (35) demonstrated that CodY represents a GTP-sensing protein that functions as a repressor under high-GTP conditions, i.e., during exponential growth in nutrient-rich medium. When *B. subtilis* cells encounter nutrient-limiting condi-

* Corresponding author. Mailing address: Institut für Mikrobiologie und Molekularbiologie, Ernst-Moritz-Arndt-Universität Greifswald, D-17487 Greifswald, Germany. Phone: 49-3834-864222. Fax: 49-3834-864202. E-mail: georg.homuth@uni-greifswald.de.

† Present address: Biotechnology Department VFB, DSM Nutritional Products Ltd., CH-4002 Basel, Switzerland.

‡ Present address: Institut für Molekulare Infektionsbiologie, University of Würzburg, D-97070 Würzburg, Germany.

tions, the cellular GTP pool drops, due either to the depletion of precursors of guanine nucleotides or to the activation of the stringent response (26). Since CodY-regulated genes are repressed during growth in media containing amino acid mixtures (2), the cellular GTP pool might be affected by amino acid availability via the stringent response due to partial amino acid limitation in minimal medium. However, recent in vitro experiments carried out in the Sonenshein laboratory demonstrated that branched-chain amino acids interact directly with CodY, thereby stimulating the binding of CodY to many of its targets (33).

In the present work, we analyzed the transcriptional organization of the genes encoding the branched-chain amino acid biosynthetic enzymes, identifying *ilvD* and *ybgE* as monocistronic transcriptional units and cotranscription of *ilvA* with the *ypmP* gene. The heptacistronic *ilvBHC-leuABCD* operon was demonstrated to exhibit posttranscriptional regulation by mRNA processing and differential segmental stabilities of the processing products, which results in different amounts of the encoded proteins.

Relatively little is known about mRNA degradation, mRNA processing, and mechanisms of posttranscriptional regulation in *B. subtilis*. In gram-negative bacteria, the extensively analyzed *pufQBALMX* operon of *Rhodobacter capsulatus* represents a model system for studying gene regulation by differential segmental mRNA stability of polycistronic operons (3, 16, 17, 23, 24). The *pufBA* genes encode the proteins of the light-harvesting I complex, while the *pufLM* genes encode the pigment-binding proteins of the reaction center. There is a 10- to 15-fold excess of light-harvesting I complexes over reaction center complexes in *R. capsulatus* cells grown under low-oxygen tension, which at least partially results from differential stabilities of the individual *puf* mRNA segments (23). As exemplified in the *puf* operon, the endoribonuclease RNase E represents a key factor in the modulation of RNA degradation and processing in gram-negative bacteria (8). In *Escherichia coli* as well as *R. capsulatus*, RNase E, the exoribonuclease PNPase, and the RNA helicase RhlB, which facilitates the unwinding of structured RNA, are organized in a large complex called the degradosome (8, 22). According to current models, degradation of the majority of the mRNAs is initiated by the binding of RNase E to the 5′ end. Subsequently, the degradosome proceeds in the 5′-3′ direction, thereby "scanning" the bound RNA for AU-rich, single-stranded RNA regions representing RNase E recognition sites. The resulting cleavage fragments are rapidly degraded by the exoribonucleases PNPase and RNase II. Both enzymes are impeded by secondary structures frequently located at the 3′ ends of primary transcripts, functioning both as transcriptional terminators and as 3′-RNA stabilizers. Therefore, the decay of structured 3′ ends is postulated to require successive rounds of addition and degradation of poly(A) tails which function as "on-ramps" for the exonucleases, particularly the PNPase. This RNA polyadenylation is performed by the poly(A) polymerase (PAPI) (8).

Although an RNase E-encoding gene cannot be derived from the genome sequence of *B. subtilis*, an RNase E-like enzymatic activity has been found (9). Whereas PNPase is present in *B. subtilis*, a gene which encodes the orthologue of PAPI is absent, although polyadenylation of mRNA has been observed (10). Obviously, the enzymatic apparatus responsible for mRNA degradation and processing differs markedly between *E. coli* and *B. subtilis*. However, the structural elements influencing mRNA stability are similar: the accessibility of 5′ and 3′ ends is crucial. Protection of the 5′ end by a stem-loop structure and frequently or strongly binding ribosomes confers stability to a particular mRNA in both species, as well as stable stem-loop structures at the 3′ end (10).

Up to now, two polycistronic operons exhibiting differential segmental mRNA stability were described in *B. subtilis*, the heptacistronic *dnaK* operon (20, 21) and the hexacistronic *gapA* operon (27, 31). In both cases, the processing of primary transcripts generates products with significantly different half-lives, resulting in different amounts of the encoded proteins. However, the identity of the endoribonucleases performing the mRNA-processing reactions is still unknown.

The *ilv-leu* operon is the third example of a polycistronic operon in *B. subtilis* exhibiting modulation of the amounts of its encoded proteins by mRNA processing and differential segmental mRNA stability. Besides regulation of the whole operon *via* CodY repression and T-box-mediated antitermination, this additional level of regulation fine-tunes the expression of its individual genes.

MATERIALS AND METHODS

Bacterial strains and growth conditions. The *B. subtilis* strains used in this study were *B. subtilis* 168 (*trpC2*) (1), PS29 (*trpC2 unkU*::*spec*), and its isogenic Δ*codY* derivative PS37 (37). All *B. subtilis* strains were grown in minimal medium (38) supplemented with glucose (0.5%) and tryptophan (16 mg/liter). If indicated, CAA (Sigma) were added to a final concentration of 0.2%. Cells were harvested in the exponential growth phase after reaching an optical density at 500 nm (OD_{500}) of 0.5.

The *ilvA*::*cat* mutant strain UM101 was constructed as follows. The complete *ilvA* coding region was amplified from *B. subtilis* 168 chromosomal DNA using *Pfu* polymerase (Stratagene) and primers ILVACLONE-5′ (5′-GGCCATGGATCCATGAAACCGTTGCTTAAAGAAAAC-3′) and ILVACLONE-3′ (5′-GGCCATGGATCCAGATTAGCAAATGGAACAAGTCCT-3′). The PCR product carried BamHI restriction sites at both ends (underlined in the primer sequences). After hydrolysis with BamHI, this fragment was inserted in BamHI-linearized pSKII(+) (Stratagene), resulting in the plasmid p*ilvA*. Subsequently, p*ilvA* was hydrolyzed using Eco47III. Using this enzyme, a 464-bp fragment was removed from the *ilvA* coding sequence, leaving 426 bp of the 5′ region and 376 bp of the 3′ region of the gene. After removal of the central 464-bp fragment, the Eco47III-hydrolyzed p*ilvA* was ligated with a 950-bp EcoRV fragment (released from pSK::*cat* [39]) carrying a chloramphenicol resistance gene with its own promoter and two transcriptional terminators, one at each end of the resistance cassette. One of the resulting plasmids, in which transcription of the *cat* and *ilvA* genes occurs in the same direction, was named p*ilvA*::*cat*. The p*ilvA*::*cat* plasmid was linearized with ScaI and used for transformation of *B. subtilis* 168, with subsequent selection on chloramphenicol-containing agar plates. One of the transformants was checked by PCR for the correct integration of the *cat* cassette in the *ilvA* locus and designated UM101.

The *ilvB*::*cat* mutant strain UM102 was constructed as follows. The complete *ilvB* coding region was amplified from *B. subtilis* 168 chromosomal DNA using *Pfu* polymerase and primers ILVBCLONE-5′ (5′-GGCCATTCTAGAATGGGGACTAATGTACAGGTGGAT-3′) and ILVBCLONE-3′ (5′-GGCCATCTCGAGAGGTTTCACCCCCACCATTTCATG-3′). The PCR product carried a XbaI restriction site at its 5′ end an a XhoI restriction site at its 3′ end (underlined in the primer sequences). After hydrolysis with XbaI and XhoI, this fragment was inserted into XbaI-XhoI-digested pBlue *Sal*I *Sma*IΔ (20), resulting in plasmid p*ilvB*. Subsequently, p*ilvB* was linearized with SmaI. Since this plasmid contains one single SmaI restriction site within *ilvB*, the hydrolysis cleaved the *ilvB* coding sequence in a 5′-terminal 581-bp fragment and a 3′-terminal 1,141-bp fragment. The SmaI-linearized p*ilvB* was ligated with the same chloramphenicol resistance cassette used for the construction of UM101. One of the resulting plasmids in which transcription of the *cat* and *ilvB* genes occurs in the same direction was chosen and named p*ilvB*::*cat*. *B. subtilis* 168 was transformed with

the *Sca*I-linearized p*ilvB*::*cat* plasmid, with subsequent selection on chloramphenicol containing agar plates. One of the transformants was checked by PCR for correct integration of the *cat* cassette in the *ilvA* locus and designated UM102.

The *B. subtilis* 168 strains carrying translational fusions of *lacZ* to the upstream regions of the *ilvA*, *ilvB*, *ilvD*, and *ybgE* genes were kindly provided by Jörg Stülke. The fusions were introduced into the *codY* null mutant strain PS37 and its isogenic wild-type strain, PS29, by transformation with chromosomal DNA and subsequent selection on agar plates containing chloramphenicol and spectinomycin. In the case of the PS37 derivative strains, the *codY* deletion was verified by PCR. In all cloning experiments, *E. coli* DH10B (Invitrogen) was used as the host strain, which was routinely grown in Luria-Bertani medium containing ampicillin (200 μg/ml) for all plasmid-bearing strains. Chloramphenicol and spectinomycin were added at 5 and 100 μg/ml, respectively.

Assay of β-galactosidase activity, RNA preparation, and Northern analysis. The β-galactosidase assay was carried out as described by Miller (32). The preparation of total RNA and the Northern hybridization procedures were carried out as described previously (13). Chemiluminescence was detected with the Lumi-Imager (Roche Diagnostics), and chemiluminographs were quantified using the Lumi-Analyse software package (Roche Diagnostics). Transcript sizes were determined by comparison with an RNA size marker (Invitrogen). The positions of the molecular size markers are depicted on the left in all Northern blot images.

The digoxigenin-labeled RNA probes were synthesized by in vitro transcription with T7 RNA polymerase and specific PCR products as templates. Synthesis of the templates by PCR was performed using the following oligonucleotide pairs: for the *ilvA* probe; ILVA-5′ (5′-ATGAAACCGTTGCTTAAAGA-3′) and ILVA-3′ (5′-CTAATACGACTCACTATAGGGAGATGTACCTACCCCAGAGAGAA-3′); for *ilvB*, ILVB-5′ (5′-ATGGGGACTAATGTACAGGT-3′) and ILVB-3′ (5′-CTAATACGACTCACTATAGGGAGATGTTGTCGGCTGGTATCCCG-3′); for *ilvC*, ILVC-5′ (5′-TATAACGGTGATATCAAAGA-3′) and ILVC-3′ (5′-CTAATACGACTCACTATAGGGAGAGCCGCAAAGAACTGCTTGCT-3′); for *ilvD*, ILVD-5′ (5′-GAGGATCACCATGGCAGAAT-3′) and ILVD-3′ (5′-CTAATACGACTCACTATAGGGAGAAGACAGTTCATTGAGTTCGC-3′); for *ilvH*, ILVH-5′ (5′-ACATTGACTGTGGTGAACCG-3′) and ILVH-3′ (5′-CTAATACGACTCACTATAGGGAGAGCTGGTTCCCCTCGCAAAAG-3′); for *leuA*, LEUA-5′ (5′-GGTCTCCGTTGCGCAAAATT-3′) and LEUA-3′ (5′-CTAATACGACTCACTATAGGGAGAGACTGCCATTCCCAAATCATC-3′); for *leuC*, LEUC-5′ (5′-ATGATGCCTCGAACAATCAT-3′) and LEUC-3′ (5′-CTAATACGACTCACTATAGGGAGAGACGTAGCCTGTGCCGAATT-3′); for *leuD*, LEUD-5′ (5′-ATGGAACCTTTGAAATCACATAC-3′) and LEUD-3′ (5′-CTAATACGACTCACTATAGGGAGAGGCTTGAAGCCAAGAGCTTC-3′); for *ybgE*, YBGE-5′ (5′-CTTCCTTGGGGTTTGGACAA-3′) and YBGE-3′ (5′-CTAATACGACTCACTATAGGGAGATGAAGACTGGCGGCATAGTT-3′); and for *ypmP*, YPMP-5′ (5′-TTGTTACTCAAAAGCCTAGA-3′) and YPMP-3′ (5′-CTAATACGACTCACTATAGGGAGACGCGTTGTGCTTTAACACCT-3′). The underlined sequences indicate the T7 promoter region.

Primer extension analysis. Primer extension was carried out as described previously (40) using the ^{32}P-labeled primer ILVC-PEX (5′-TTCAGGGCATGTGCGTGGCC-3′). The DNA-sequencing reactions were carried out with the same primer and an 1,567-bp *ilvH-ilvC* DNA template which was generated by PCR using the primer pair ILVH-5′B (5′-CTAATACGACTCACTATAGGGAGATTGAAAAGAATTATCACATT-3′) and ILVC-3′B (5′-ATTTTGCGCAACGGAGACCA-3′).

Preparation of protein extracts and 2-D protein gel electrophoresis. *B. subtilis* strain 168 growing in minimal medium at 37°C was harvested in the exponential growth phase after reaching an OD_{500} of 0.5. Protein extracts were prepared as described previously (5). IPG strips in the pH range from 4 to 7 (Amersham Biosciences) were loaded with 100 μg of crude protein extract. Isoelectric focusing using the Multiphor II unit (Amersham Biosciences) and sodium dodecyl sulfate polyacrylamide gel electrophoresis using the Investigator two-dimensional (2-D) electrophoresis system (Genomic Solutions) were performed as described previously (5). The resulting 2-D gels were fixed with 50% (vol/vol) methanol–7% (vol/vol) acetic acid and stained with SYPRO Ruby protein gel stain (Molecular Probes). Fluorescence was detected using a Storm860 imager (Molecular Dynamics). The 2-D gel image analysis and quantification of the protein amounts were performed with the Delta 2-D software (Decodon). Protein extracts from three independent cultures were used for quantification, and each sample was resolved twice. The identification of proteins was performed by matrix-assisted laser desorption ionization-time of flight (MALDI-TOF) mass spectrometry as described previously (5).

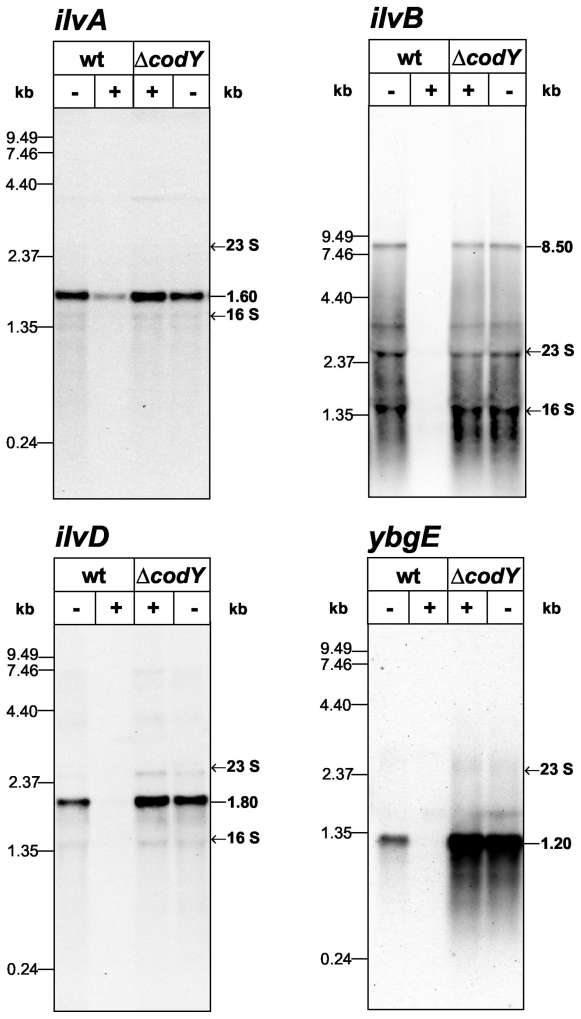

FIG. 1. Northern analysis of *ilvA*, *ilvB*, *ilvD*, and *ybgE* in PS29 (wt) and PS37 (Δ*codY*). RNA was prepared from cells growing exponentially in minimal medium in the presence (+) or absence (−) of CAA (0.2%). Electrophoretic separation of the RNA (5 μg per lane) was performed using 1.2% (*ilvA*, *ilvD*, and *ybgE*) or 0.6% (*ilvB*) agarose gels.

RESULTS

Analysis of regulation and transcriptional organization of the genes encoding the branched-chain amino acid biosynthetic enzymes. The results of our global gene expression analysis of *B. subtilis* grown in minimal medium with and without CAA (29) prompted us to conclude that CodY-dependent regulation of the genes for the biosynthesis of branched-chain amino acids (*ilv-leu* operon, *ilvA*, *ilvD*, and *ybgE*) was occurring. To verify this hypothesis and to obtain information about the transcriptional organization of these genes, Northern analyses using probes with specificity for *ilvA*, *ilvB*, *ilvD*, and *ybgE* were carried out. To this end, RNA was prepared from *B. subtilis* PS29 and the isogenic Δ*codY* mutant PS37 grown in minimal medium in the presence or absence of CAA until the OD_{500} reached 0.5. The results are given in Fig. 1. The *ilvA*-specific probe detected a single mRNA of around 1.6 kb, indicating contranscription of *ilvA* and the downstream gene

ypmP. The *ilvB* Northern blot demonstrated a large (8.5-kb) mRNA predicted to encompass the coding regions of *ilvB*, *ilvH*, *ilvC*, *leuA*, *leuB*, *leuC*, and *leuD*. The *ilvD* and *ybgE* genes were found to be monocistronically transcribed as mRNAs of 1.8 and 1.2 kb, respectively.

As shown in Fig. 1, significantly smaller amounts of *ilvA*, *ilvB*, *ilvD*, and *ybgE* mRNA were observed in the wild type in presence of CAA whereas similar amounts of mRNA were detected under both growth conditions in the *codY* mutant. In agreement with the study by Molle et al. (33), these results demonstrated CodY-dependent regulation of the branched-chain amino acid biosynthesis genes. However, the extent of CodY repression was different: whereas no *ilvB*, *ilvD*, and *ybgE* specific transcripts were detected in the wild type in the presence of CAA, a faint band was visible for *ilvA*, indicating weaker CodY repression. Furthermore, the *ilvA*, *ilvB*, and *ilvD* specific mRNAs were present in comparable amounts in the wild-type strain in the absence of CAA and in the *codY* mutant. In contrast, the amount of *ybgE* mRNA was significantly larger in the mutant strain. This indicated that in wild-type cells, CodY strongly represses the *ybgE* gene even in minimal medium without CAA. These results were confirmed by β-galactosidase activity assays of wild-type and Δ*codY* strains carrying chromosomal *lacZ* fusions to the *ilvA*, *ilvB*, *ilvD*, and *ybgE* promoter regions with samples taken under the same growth conditions as for the Northern blot analyses (data not shown).

Analysis of the transcriptional units carrying the genes encoding the branched-chain amino acids biosynthesis enzymes after GTP depletion. It was previously shown that the CodY repressor is active under conditions of high cellular GTP concentration (35). Consequently, GTP depletion causes derepression of CodY-regulated genes. Ratnayake-Lecamwasam et al. (35) demonstrated induction of the CodY-repressed *dpp* operon by treatment of cells with decoyinine, a GMP synthetase inhibitor. In the present study, mycophenolic acid, which inhibits the IMP dehydrogenase and thus the synthesis of guanine nucleotides, was used to decrease the cellular GTP pool. Cultures of *B. subtilis* PS29 and the isogenic Δ*codY* mutant PS37 were grown in minimal medium with CAA. When the OD_{500} had reached 0.5, mycophenolic acid was added to a final concentration of 100 μM. Samples for RNA preparation were removed before and 10, 20, and 40 min after addition of mycophenolic acid. The RNA preparations were used in Northern hybridizations with *ilvA*-, *ilvB*-, *ilvD*-, and *ybgE*-specific probes (Fig. 2).

The *ilvA*-, *ilvB*-, and *ilvD*-specific mRNAs were significantly upregulated in the wild type by 10 min after addition of mycophenolic acid. However, the derepressed wild-type mRNA levels did not reach that of the *codY* mutant before mycophenolic acid treatment, although the amount of *ilvA* mRNA was very similar to that of the mutant. In the *codY* mutant strain, neither the *ilvA*- nor the *ilvB*- and *ilvD*-specific mRNAs were induced on mycophenolic acid addition. In contrast, the amounts of mRNA were significantly reduced, most obviously in the case of *ilvB*. Whereas CodY-dependent derepression of *ilvA*, *ilvB*, and *ilvD* could be confirmed following GTP depletion, the monocistronic *ybgE* exhibited a different pattern of expression. Although *ybgE* was clearly CodY dependent, it remained strongly repressed after mycophenolic acid treatment and was not induced by GTP depletion. The expression of chromosomal fusions between *lacZ* and the promoter regions of *ilvA*, *ilvB*, *ilvD*, and *ybgE*, measured before and 40 min after the addition of mycophenolic acid, confirmed the results of the Northern blot analyses (data not shown).

Northern blot analysis of *ypmP* and *ilvC*. The results of the Northern hybridizations demonstrated single monocistronic *ilvD* and *ybgE* mRNAs, whereas a bicistronic *ilvA-ypmP* mRNA and a heptacistronic *ilv-leu* mRNA could be predicted. To complete the analysis of the two polycistronic operons, RNA prepared from the wild type (PS29) and Δ*codY* mutant (PS37), after growth in minimal medium in the presence or absence of CAA, was used in Northern hybridizations with *ypmP*- and *ilvC*-specific probes (Fig. 3). In addition to the 1.6-kb *ilvA-ypmP* mRNA, which was already demonstrated using the *ilvA* probe, the *ypmP* probe detected an additional mRNA of 0.25 kb, which exhibited the expression pattern of *ilvA*. This monocistronic *ypmP* mRNA was present in larger amounts compared to the bicistronic transcript. For *ilvC*, two further mRNAs were detected in addition to the 8.5-kb mRNA, one of around 5.8 kb and one of 1.2 kb. The 5.8-kb mRNA was present in larger amounts than the 8.5-kb mRNA, and the 1.2-kb mRNA was the most abundant transcript. All three mRNA species detected with the *ilvC* probe had the same expression pattern. The newly identified mRNA species could be generated by endoribonucleolytic processing of the 1.6-kb *ilvA-ypmP* mRNA and the 8.5-kb *ilv-leu* mRNA or by the activities of additional internal promoters. To differentiate between these possibilities, several experiments were carried out.

Detection of an internal promoter upstream of *ypmP*. The results obtained with strain PS29 and the isogenic Δ*codY* mutant PS37 concerning the regulation of the four transcriptional units as well as all detected mRNA species were reproducible in the *B. subtilis* 168 background. Since this strain is routinely used in our laboratory, all further experiments were carried out with *B. subtilis* 168. To analyze the origin of the 0.25-kb *ypmP* mRNA, a mutant was constructed to separate *ypmP* transcription from the *ilvA* promoter. Therefore, part of the *ilvA* coding region was replaced by a chloramphenicol resistance cassette carrying its own promoter and two transcriptional terminators, as described in Materials and Methods (Fig. 4). If the 0.25-kb *ypmP* mRNA was generated by endoribonucleolytic cleavage of the 1.6-kb *ilvA-ypmP* mRNA, it should be absent when transcription from the promoter upstream of *ilvA* is blocked. However, if an internal promoter upstream of *ypmP* was responsible for the synthesis of the 0.25-kb mRNA, this should be present even when the *ypmP* gene and the *ilvA* promoter were uncoupled. RNA was prepared from the *ilvA* mutant and from the *B. subtilis* 168 wild type growing exponentially in minimal medium supplemented with 1 mM isoleucine or CAA. Growth of the *ilvA* mutant requires isoleucine due to the loss of the threonine dehydratase activity. These RNA preparations were used in Northern experiments using *ilvA*- and *ypmP*-specific probes (Fig. 4).

Both probes detected the 1.6-kb *ilvA-ypmP* mRNA in the wild-type strain but not in the *ilvA* mutant, demonstrating the uncoupling of *ypmP* transcription from the *ilvA* promoter. In the *ilvA* mutant, the *ilvA* probe additionally hybridized to an mRNA of 0.4 kb that showed the same regulatory pattern as the 1.6-kb mRNA of the wild type. This transcript most probably results from transcription initiation at the *ilvA* promoter

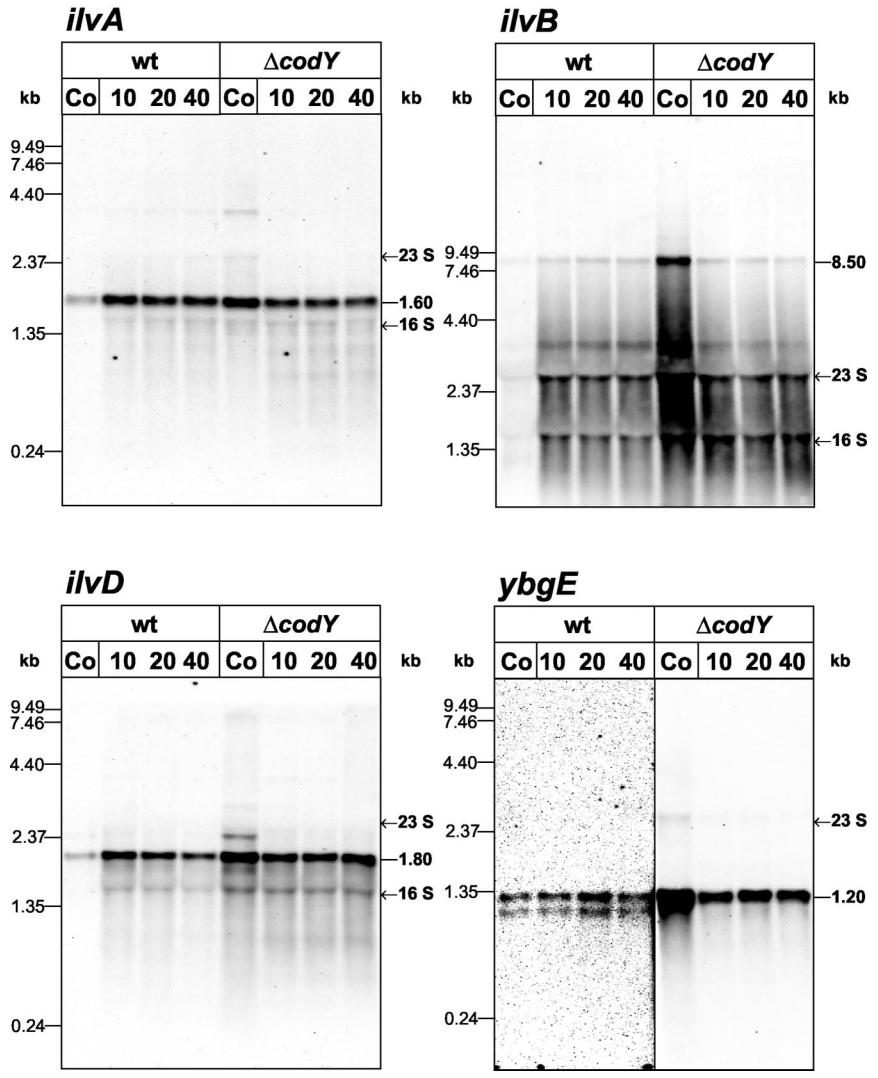

FIG. 2. Northern analysis of *ilvA*, *ilvB*, *ilvD*, and *ybgE* under conditions of GTP depletion. PS29 (wt) and PS37 (Δ*codY*) were grown in minimal medium in the presence of CAA (0.2%). After the culture reached an OD_{500} of 0.5, mycophenolic acid (Sigma) was added to a final concentration of 100 μM. RNA was prepared from cells harvested before (Co [control]) and at the indicated times (10, 20, and 40 min) after the addition of mycophenolic acid. Electrophoretic separation of the RNA (5 μg per lane) was performed using 1.2% (*ilvA*, *ilvD*, and *ybgE*) or 0.6% (*ilvB*) agarose gels. Note that in the case of the *ybgE* luminograph, different exposure times for the wild-type and Δ*codY* strains were used. Whereas a long exposure time was necessary to detect the wild-type bands, the very strong signals in the Δ*codY* strain required a short exposure time to avoid overexposition.

and termination at the first terminator within the chloramphenicol resistance cassette. However, the 0.25-kb *ypmP* mRNA was still present in the mutant strain, clearly indicating the presence of an additional promoter immediately upstream of *ypmP*, which is likely to be located in the relatively large intercistronic region of 89 bp between *ilvA* and *ypmP* (Fig. 4). Thus, generation of the 0.25-kb mRNA by mRNA processing could be excluded. Since this transcript still exhibited CAA-dependent regulation, the *ypmP* promoter might also be under CodY control.

Detailed Northern analysis of the *ilv-leu* operon. To unravel the transcriptional organization of the *ilv-leu* operon, a comprehensive Northern analysis was carried out. Wild-type cells grown in minimal medium were harvested during exponential growth (OD_{500} of 0.5) for RNA preparation. This RNA was hybridized to probes with specificity for *ilvB*, *ilvH*, *ilvC*, *leuA*, *leuC*, and *leuD* (Fig. 5A). The *ilvB* and *ilvH* probes detected exclusively the 8.5-kb mRNA encompassing the entire operon. As shown above, the *ilvC* probe detected the 8.5-, 5.8-, and 1.2-kb mRNAs. The *leuA* probe hybridized to the 8.5- and 5.8-kb mRNAs and, with much lower efficiency than the *ilvC* probe, to the 1.2-kb mRNA. Finally, the *leuC*- and *leuD*-specific probes detected only the two large mRNA species.

These results are summarized in Fig. 5C. The 8.5-kb mRNA initiated at the promoter upstream of *ilvB* is terminated at the two transcriptional terminators downstream of *leuD*. The 5′ end of the 5.8- and 1.2-kb mRNAs is predicted to be located close to the 5′ end of *ilvC* or the 3′ end of *ilvH*. Finally, the 3′ end of the 1.2-kb mRNA is predicted to be located in the 5′-proximal part of the *leuA* coding region. Indeed, a signifi-

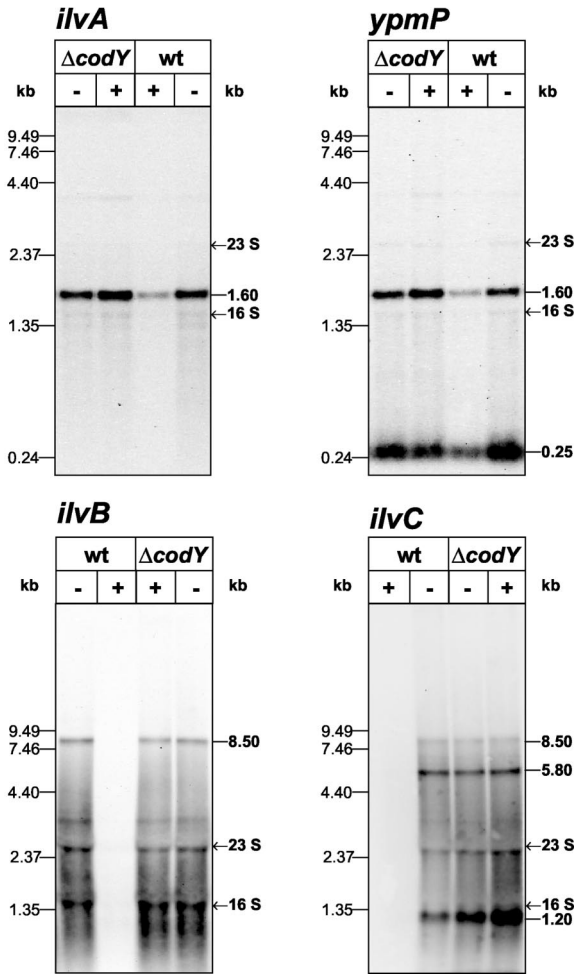

FIG. 3. Northern analysis of *ilvA*, *ypmP*, *ilvB*, and *ilvC* in PS29 (wt) and PS37 (Δ*codY*). RNA was prepared from cells growing exponentially in minimal medium in the presence (+) or absence (−) of CAA (0.2%). Electrophoretic separation of the RNA (5 μg per lane) was performed using 1.2% (*ilvA* and *ypmP*) or 0.6% (*ilvB* and *ilvC*) agarose gels.

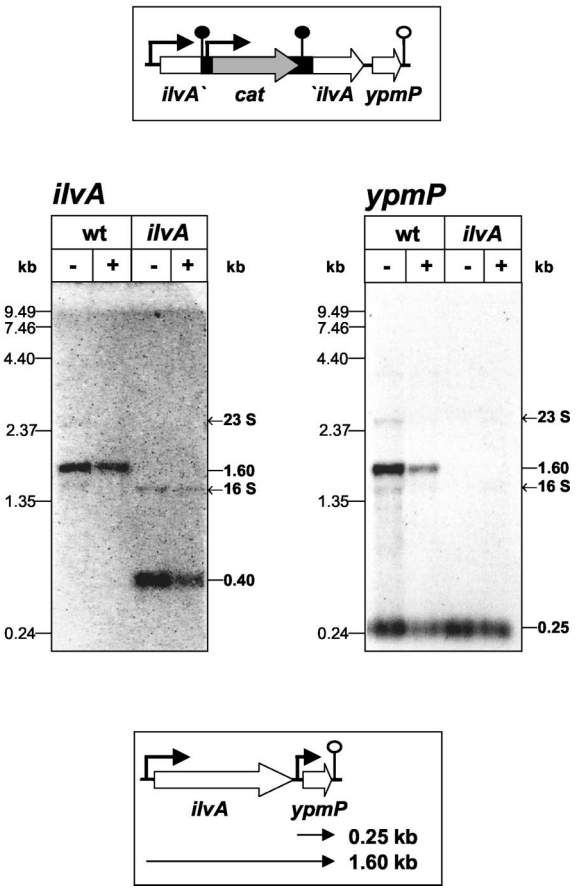

FIG. 4. Northern analysis of the *ilvA*::*cat* mutant strain UM101. RNA was prepared from UM101 (*ilvA*) and *B. subtilis* 168 (wt) growing exponentially in minimal medium supplemented with 1 mM isoleucine in the presence (+) or absence (−) of CAA (0.2%). RNA electrophoresis (5 μg per lane) was performed using 1.2% agarose gels. Hybridization was carried out using *ilvA*- and *ypmP*-specific probes. The top drawing shows the chromosomal organization of the *ilvA-ypmP* locus in UM101. The detected transcriptional organization of the wild-type locus is depicted in the bottom drawing.

cant secondary structure can be derived from the DNA sequence at the 5′ end of *leuA* (Fig. 5B). This putative stem-loop structure ($\Delta G = -16$ kcal/mol) is located around 120 bases downstream of the *leuA* start codon. Whereas this secondary structure could explain the generation of the 3′ end of the 1.2-kb mRNA by partial transcriptional termination or by stalling of exoribonucleases, the origin of the 5′ end of 1.2- and 5.8-kb mRNA remained to be detected. As with the *ilvA-ypmP* operon, this 5′ end could be generated by endoribonucleolytic mRNA processing or by the activity of an internal promoter.

Detection of an mRNA-processing event within the *ilv-leu* operon. To differentiate between the activity of an internal promoter and an mRNA-processing event, uncoupling of all downstream located genes from the *ilvB* promoter was achieved by insertion of the chloramphenicol resistance cassette into the 5′ half of the *ilvB* coding region as described in Materials and Methods (Fig. 6). *B. subtilis* 168 and the isogenic *ilvB* mutant strain were grown in minimal medium in the presence of CAA to overcome the auxotrophy of the mutant strain. For RNA preparation, cells were harvested during exponential growth (OD_{500} of 0.5). In a Northern experiment, these RNA preparations were hybridized with an *ilvC*-specific probe (Fig. 6). Whereas the corresponding RNA gel showed the good quality of the RNA preparations, the luminograph of the Northern hybridization unambiguously demonstrated the absence of *ilvC*-specific mRNAs in the mutant strain. This result revealed that the complete *ilv-leu* operon is inactivated in the *ilvB* mutant. Consequently, the 5.8- and 1.2-kb mRNAs are generated by endoribonucleolytic mRNA processing of the 8.5-kb mRNA and not by the activity of an internal promoter.

Mapping of the mRNA-processing site upstream of *ilvC* by primer extension. To determine the mRNA cleavage site upstream of *ilvC*, a primer extension experiment was carried out using RNA prepared from *B. subtilis* 168 grown in minimal medium in the presence or absence of CAA. These RNA preparations were hybridized to a radioactively labeled primer complementary to the *ilvC*-specific mRNA, 113 bases downstream of the *ilvC* start codon. The result of the primer exten-

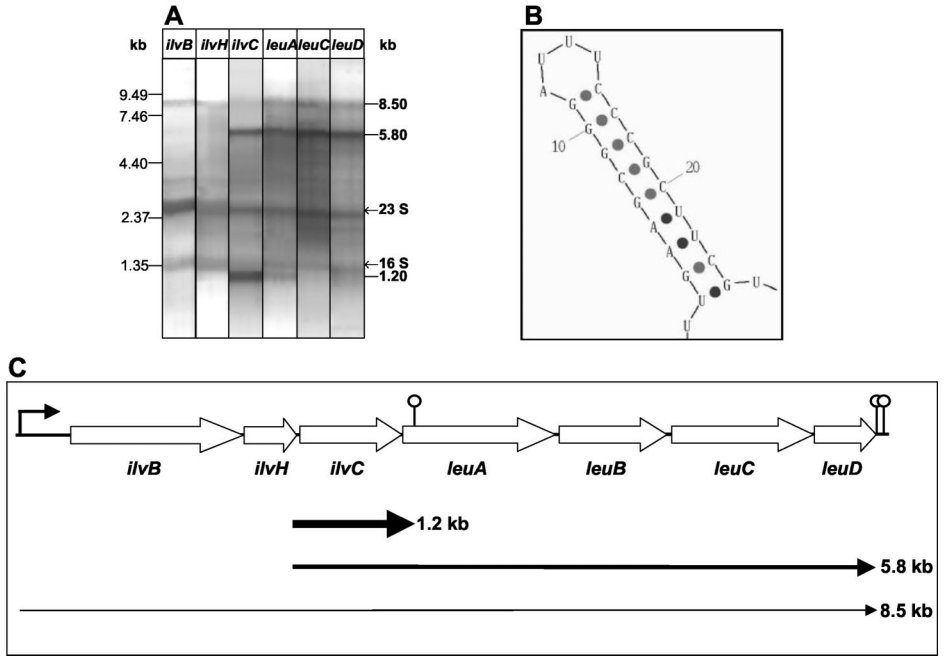

FIG. 5. Detection of mRNAs specified by the *ilv-leu* operon. (A) Northern analysis. RNA was prepared from *B. subtilis* 168 growing exponentially in minimal medium. Six slots of a 0.6% RNA gel were loaded in parallel with 5 μg of this preparation. After electrophoresis and blotting, the membrane was cut into six strips, which were subsequently hybridized to probes with specifity for *ilvB*, *ilvH*, *ilvC*, *leuA*, *leuC*, and *leuD*. The reassembled chemiluminographs are shown. (B) Secondary structure ($\Delta G = -16$ kcal/mol) in the 5′-terminal region of *leuA* as predicted by the Zuker algorithm (43). (C) Transcriptional organization of the *ilv-leu* operon as derived from the Northern analysis. The lengths of the different transcripts are indicated. The thickness of the arrows reflects the abundance of the transcripts.

sion experiment is shown in Fig. 7A. One single mRNA 5′ end was mapped, corresponding to a G residue located 92 bases upstream of the *ilvC* start codon within the *ilvH* coding region, 66 bases upstream of the *ilvH* stop codon (Fig. 7B). The sequencing reaction of the *ilvH-ilvC* PCR product revealed an additional C residue 46 bp upstream of the 3′ end of the *ilvH* coding region which was lacking in the published sequence (25). This was confirmed by sequencing two independently generated PCR products. This insertion (indicated in Fig. 7B) changes the C-terminal amino acid sequence of IlvH from

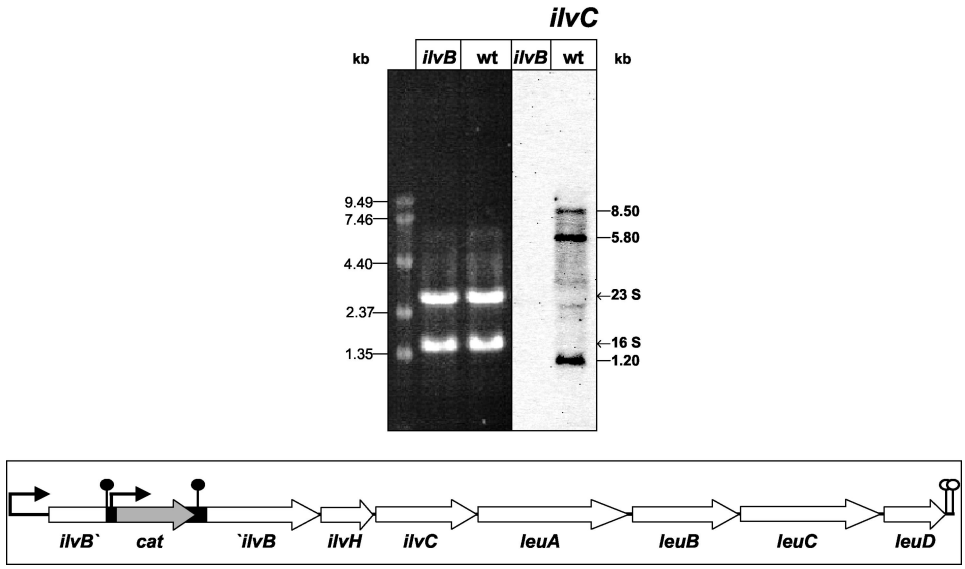

FIG. 6. Northern analysis of the *ilvB*::*cat* mutant strain UM102. RNA was prepared from UM102 (*ilvB*) and *B. subtilis* 168 (wt) growing exponentially in minimal medium in the presence of CAA (0.2%). This RNA preparation (5 μg per lane) was electrophoretically separated in a 0.6% agarose gel, which is shown on the left side. The corresponding chemiluminograph after hybridization of the blotted RNA with an *ilvC* probe is depicted on the right side. The drawing shows the chromosomal organization of the *ilv-leu* locus in UM102.

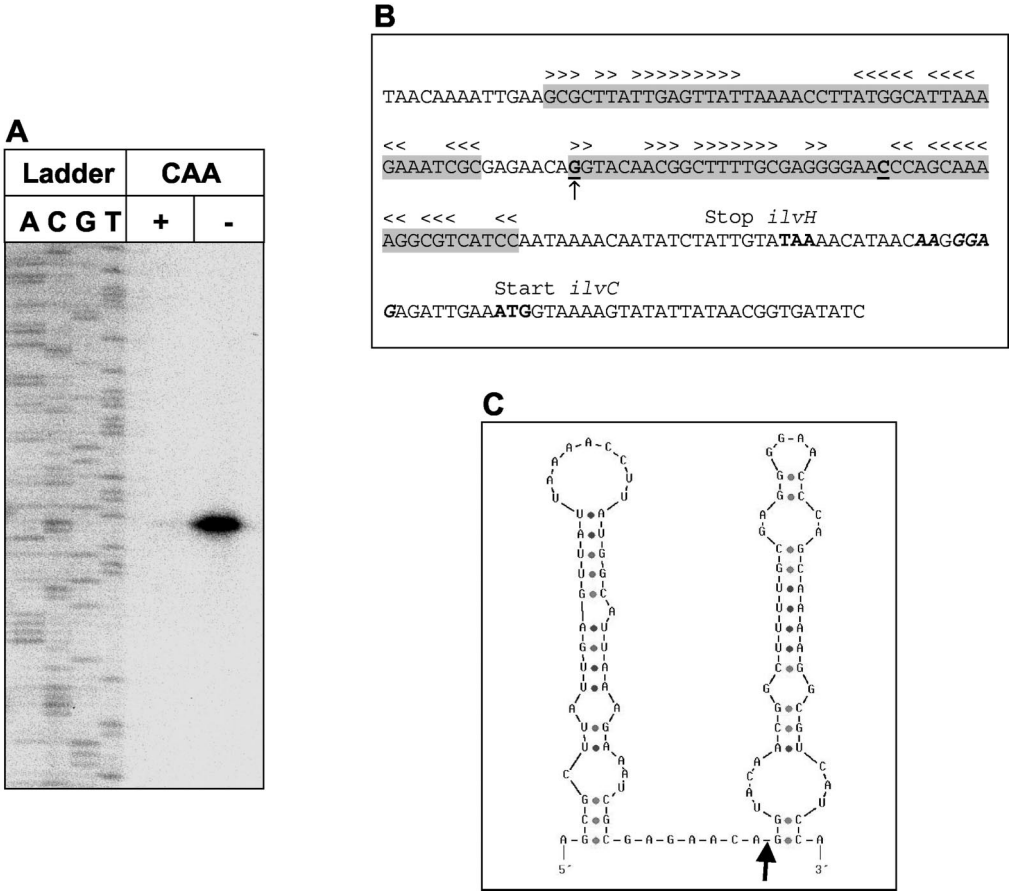

FIG. 7. Mapping of the mRNA-processing site upstream of *ilvC*. (A) Primer extension analysis. The reactions were performed using 5 μg of RNA prepared from *B. subtilis* 168 growing exponentially in minimal medium in the presence (+) or absence (−) of CAA (0.2%). Lanes A, C, G, and T show the dideoxy sequencing ladder obtained with the same primer as used for the primer extension reactions. (B) Sequence of the chromosomal region surrounding the mapped processing site. Regions predicted to specify secondary structures on the mRNA level are highlighted in grey, and stem-loop structures are depicted as arrowheads. The C residue absent in the published genome sequence is underlined and in boldface, and the G residue representing the mapped 5′ end is marked by an arrow. The *ilvH* stop codon and the *ilvC* start codon are shown in boldface, and the *ilvC* ribosome-binding site is shown in italic. (C) Secondary-structure prediction for the mRNA surrounding the processing site according to the Zuker algorithm (43). The mapped mRNA cleavage site is indicated by an arrow.

SKRRHPIKQYLLYKT to QQKASSNKTISIV, resulting in a protein shortened by 2 amino acids.

The signal representing the mapped 5′ end exhibited the expected regulatory pattern (Fig. 7A). To test for a nonspecific reverse transcriptase product, the primer extension was performed in parallel using *ilvH-ilvC* RNA generated by in vitro transcription. In this control reaction, no significant signal appeared at the position of the mapped 5′ end (data not shown). To obtain more information about the structural determinants of the mapped processing site, the surrounding mRNA region was folded in silico by using the Zuker algorithm (43). This reveals that the mRNA cleavage site is located between an A and a G residue directly upstream of a relatively stable complex secondary structure ($\Delta G = -19.0$ kcal/mol), at the distal 3′ site of a single-stranded mRNA stretch of 7 bases (Fig. 7C). The single-stranded region is flanked at the 3′ side by the above-mentioned secondary structure and at the 5′ side by an additional, less stable secondary structure ($\Delta G = -3.0$ kcal/mol) at the 5′ side. After cleavage, the 5′ ends of the resulting processing products are located within a base-paired double-stranded region. Since it is known that 5′ base-paired ends of mRNA confer protection against degradation in *E. coli* as well as *B. subtilis* (10), it could be predicted that the 5.8- and 1.2-kb processing products are more stable than the 8.5-kb precurser. This assumption was further strengthened by the observation that the processing products are present in the cell in larger amounts than is the full-length precursor mRNA, as revealed by the Northern analyses. Therefore, it was tempting to speculate that the physiological function of the processing event was the generation of mRNAs with higher stabilities. This prediction was tested by half-life determination of the 8.5-, 5.8-, and 1.2-kb mRNAs.

Half-life determination of the three mRNA species of the *ilv-leu* operon. Rifampin was added to exponentially growing *B. subtilis* 168 cells to prevent the initiation of transcription. Samples for RNA preparation were removed before and at different times after the rifampin addition. These RNA samples were hybridized in Northern experiments with *ilvB*- and *ilvC*-specific probes (Fig. 8). Quantification of the resulting luminographs allowed the calculation of specific half-lifes: for the

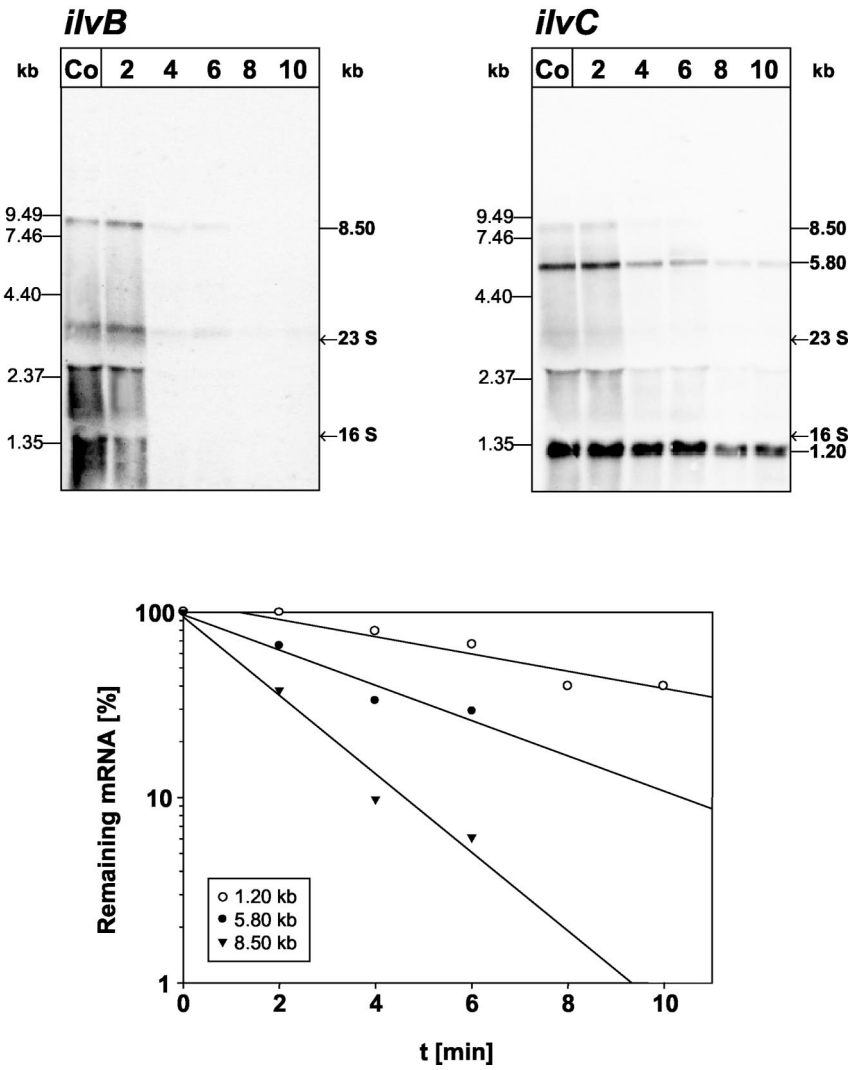

FIG. 8. Half-life determination of the different mRNAs of the *ilv-leu* operon. RNA (5 μg per lane) was prepared from *B. subtilis* 168 growing exponentially in minimal medium before (Co) and at different times (given in minutes) after the addition of rifampin. After RNA electrophoresis in 0.6% agarose gels and blotting, the membranes were hybridized to *ilvB*- and *ilvC*-specific probes. The half-lifes of the 8.5-, 5.8-, and 1.2-kb mRNA were determined by linear regression analysis plots of the percentage of remaining mRNA versus the time. The half-life data were obtained from three experiments using independently prepared RNA.

8.5-kb primary transcript, a half-life of 1.2 min was determined, whereas the 5.8- and 1.2-kb processing products exhibited half-lifes of 3.0 and 7.6 min, respectively. Thus, the postulated differential mRNA stabilities resulting from the different 5′ ends of the primary transcript and the processing products were verified.

The mRNA analyses showed that the *ilvB* and *ilvH* genes encoding the acetolactate synthase subunits are expressed only as part of the 8.5-kb mRNA and specify the smallest amounts of mRNA of all genes in the operon. The mRNA-processing event upstream of *ilvC*, which generates the 5.8- and 1.2-kb mRNAs, should also result in the generation of a 5′-proximal processing product of around 2.7 kb containing *ilvB* and the truncated *ilvH*. It is possible that the faint band above the nonspecific 23 S rRNA signal, which was detected with the *ilvB*-specific probe, represents this processing product (Fig. 1, 2, 3, 5, and 8). However, the detection of this mRNA was not reliably reproducible since the band was absent in several RNA preparations, pointing to a very low mRNA stability. The *leuA*, *leuB*, *leuC*, and *leuD* genes, encoding 2-isopropylmalate synthase, 3-isopropylmalate dehydrogenase, and the 3-isopropylmalate dehydratase subunits, respectively, are expressed as part of the 8.5- and 5.8-kb mRNA. Consequently, these genes specify more mRNA than do *ilvB* and *ilvH*. The largest amount of mRNA is specified by *ilvC*, encoding ketol-acid reductoisomerase, which is expressed as part of three mRNA species. In addition to the 8.5- and 5.8-kb mRNAs, *ilvC* specifies the 1.2-kb mRNA which represents the most abundant transcript. These observations raised the question whether the different amounts of mRNA are also reflected in the amounts of proteins synthesized. Therefore, the relative amounts of the proteins encoded by the operon were compared.

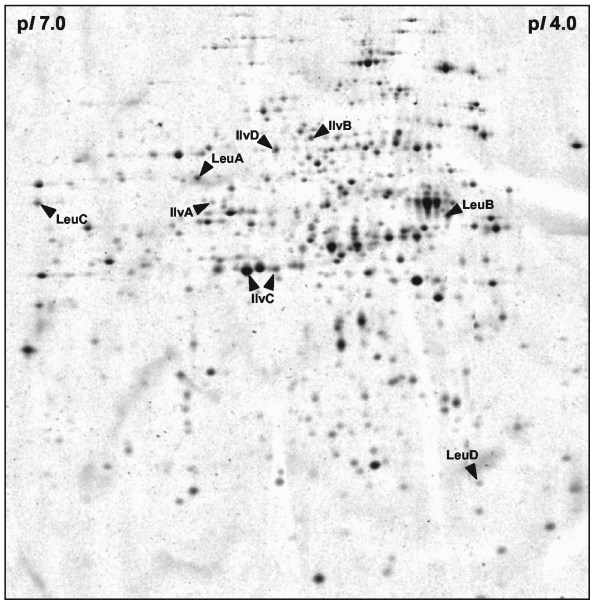

FIG. 9. SYPRO ruby-stained cytosolic proteins of *B. subtilis* 168 separated by 2-D protein gel electrophoresis. The protein extract (100 μg) prepared from cells growing exponentially in minimal medium was separated in a pH gradient of 4 to 7. The labeled spots represent proteins involved in the biosynthesis of branched-chain amino acids.

Determination of the relative protein amounts of the enzymes encoded by the *ilv-leu* operon. To determine the relative cellular amounts of the proteins involved in branched-chain amino acid biosynthesis, protein extracts were prepared from *B. subtilis* 168 grown in minimal medium. These extracts were separated by 2-D polyacrylamide gel electrophoresis and stained with SYPRO Ruby protein gel stain (Fig. 9). Following quantification of the 2-D gel images, the relative amounts of the IlvB, IlvC, LeuA, LeuB, LeuC, and LeuD proteins could be calculated; IlvH was not detectable in the 2-D gels in the pH range from 4 to 7 due to its alkaline isoelectric point (pI). However, since IlvB and IlvH form a heteromer and are translationally coupled (the *ilvB* stop codon and the *ilvH* start codon share two bases), it can be postulated that the two proteins are present in similar amounts. The averaged quantification data revealed the following relative proteins amounts: 1.2 ± 0.16 (IlvB), 11.76 ± 1.0 (IlvC), 1.72 ± 0.20 (LeuA), 1.72 ± 0.22 (LeuB), 1.12 ± 0.25 (LeuC), and 1.0 ± 0.23 (LeuD). Thus, the large amount of *ilvC*-specific mRNA, which is caused primarily by the remarkably long half-life of the 1.2-kb processing product, is indeed reflected by a correspondingly large amount of the IlvC protein. Whereas the monomeric species of the other proteins encoded by the *ilv-leu* operon were detected in comparable amounts, the abundance of IlvC was around 10-fold higher. However, there was no difference between the amounts of the proteins encoded by *ilvB* showing the smallest mRNA amount of the operon and *leuA*, *leuB*, *leuC*, and *leuD*, exhibiting mean mRNA amounts. In addition to the proteins encoded by the *ilv-leu* operon, the IlvA and IlvD proteins were analyzed. Whereas the amount of IlvD (1.28 ± 0.23) was comparable to IlvB, LeuA, LeuB, LeuC, and LeuD, the IlvA protein was present in significantly smaller amounts (0.36 ± 0.03).

DISCUSSION

In the present study, the transcriptional organization and regulation of the genes encoding the branched-chain amino acid biosynthetic enzymes were analyzed. As already reported by Molle et al. (33), the *ilv-leu* operon and the *ilvA*, *ilvB*, and *ybgE* genes were shown to be controlled by the global transcriptional regulator, CodY. However, it is still not known why the branched-chain amino acid biosynthetic pathway is coregulated with early-stationary-phase and sporulation genes in response to the nutritional state of the cell. Possibly, CodY regulation of branched-chain amino acid biosynthesis occurs because spore formation requires de novo biosynthesis of fatty acids (36). Valine, leucine, and isoleucine are the precursors for biosynthesis of iso- and anteiso-branched fatty acids, which represent the major fatty acid species of the membrane lipids in *Bacillus* species (11). The absence of de novo fatty acid biosynthesis at the onset of sporulation results in a block of σ^E-directed gene expression in the mother cell, caused by the failure of pro-σ^E processing to its active form (36). It was suggested that de novo fatty acid biosynthesis contributes to the specific phospholipid composition of the mother cell, which is predicted to be essential for activation of the pro-σ^E processing protease, SpollGA (36). Therefore, CodY-mediated induction of branched-chain amino acid biosynthesis genes would ensure the availability of precursors for de novo fatty acid biosynthesis at the onset of sporulation.

The most interesting results of this study were obtained in the context of the posttranscriptional regulation of the *ilv-leu* operon. This operon is transcribed from a single promoter which is located upstream of *ilvB*. The corresponding transcriptional start site was mapped 482 bases upstream of the *ilvB* start codon (14). The large leader region mediates regulation of the *ilv-leu* operon by antitermination via the T-box mechanism (14, 30). A full-length 8.5-kb primary transcript is synthesized by transcriptional initiation at the *ilvB* promoter and termination at one of the two terminator structures (ΔG = −19.8 and −12.7 kcal/mol), which can be derived from the sequence immediately downstream of *leuD*. The processing event upstream of *ilvC* generates different processing products: a 5′-proximal product of around 2.7 kb containing *ilvB* and the truncated *ilvH* is postulated to exhibit a very low stability. Removal of the 5′ portion of the 8.5-kb mRNA generates the new 5′ end of the 5.8-kb as well as the 1.2-kb mRNA, which results in significantly more stable processing products.

Possibly, partial transcriptional termination occurs at the stem-loop structure in the 5′-terminal region of the *leuA* coding sequence (Fig. 5B). This would result in a primary transcript of around 3.9 kb, which should be detectable using *ilvB*, *ilvH*, and *ilvC* probes. However, a corresponding band was not detected, suggesting a very short half-life of this postulated primary transcript. Rapid processing at the site upstream of *ilvC* may prevent the accumulation of detectable amounts of mRNA. Alternatively, the secondary structure in the 5′-terminal region of *leuA* may not function primarily as a transcriptional terminator but as a 3′ mRNA-stabilizing element. Accordingly, the 1.2-kb processing product is generated by endoribonucleolytic cleavage of the 8.5-kb precurser at the processing site upstream of *ilvC* and exonucleolytic degradation of the 8.5- and 5.8-kb mRNAs, which is impeded at the

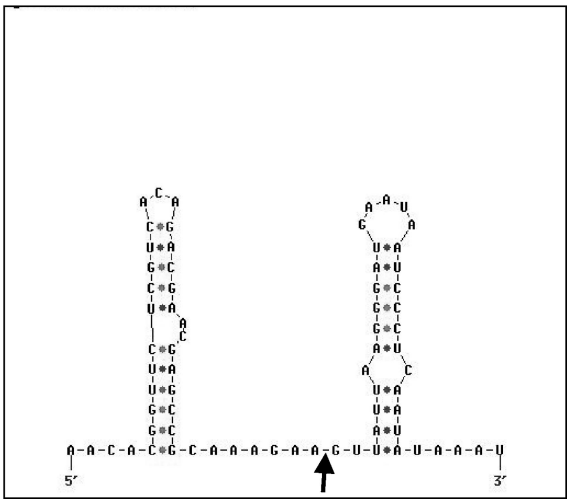

FIG. 10. The mRNA secondary structures surrounding the processing site mapped in the *gapA* operon (27). The mapped mRNA cleavage site is indicated by an arrow.

stem-loop structure downstream of *ilvC*. The latter assumption is further strengthened by the fact that despite sharing an mRNA 5′ end, the 5.8-kb processing product has a significantly shorter half-life (3.0 min) than does the 1.2-kb product (7.6 min). The strong secondary structures formed by the terminators downstream of *leuD* can be predicted to protect the distal 3′ end of the 8.5- and 5.8-kb mRNAs against exoribonucleolytic degradation. Since exoribonucleases require unpaired single-stranded 3′ ends to attach to the mRNA, recognition sites for endoribonucleases able to generate such 3′ ends have to be postulated in the region between the secondary structure downstream of *ilvC* and the farthest 3′ end of the operon. Finally, we cannot exclude the possibility that this secondary structure functions as both a 3′ mRNA stabilizer and a transcriptional terminator.

The processing site upstream of *ilvC* is of especial interest. The secondary-structure prediction for this mRNA region resembles the one of the processing site mapped in the *cggR-gapA-pgk-tpi-pgm-eno* operon (*gapA* operon) at the farthest 3′ end of the *cggR* coding region (27). As shown in Fig. 7C and 10, mRNA cleavage occurs in both cases between A and G residues within single-stranded regions flanked by stem loop structures, near the downstream stem-loop. Single-stranded, mostly AU-rich RNA regions which are stabilized by adjacent stem-loop structures represent recognition sites for the most important *E. coli* endoribonuclease RNase E (8). An enzymatic activity similar to RNase E was described in *B. subtilis* (9), although the corresponding gene is absent from the genomic sequence (25). This postulated RNase E-like *B. subtilis* enzyme, whose gene still remains to be identified, might be responsible for the endoribonucleolytic processing of the *gapA* and *ilv-leu* operons.

In both cases, the processing events generate products with different mRNA stabilities. Due to its very low stability, the 5′-proximal *ilvBH* processing product of the *ilv-leu* operon could not be be detected reliably whereas the 3′-proximal 1.2- and 5.8-kb processing products exhibited higher stabilities (half-lives of 7.6 and 3.0 min, respectively). The 5′-proximal processing product of the *cggR-gapA-pgk-tpi-pgm-eno* operon, which encompasses the leader region and a 3′-truncated *cggR* coding sequence, exhibited a half-life of 1.5 min, whereas the 3′-proximal 1.2-kb *gapA*-processing and 6.2-kb *gapA-pgk-tpi-pgm-eno*-processing products showed half-lives of 3.5 and 3.0 min, respectively. The more stable 3′-proximal processing products of the *ilv-leu* and *gapA* operons have a common structural feature: the processing events generate 5′ ends which are characterized by complex secondary structures. In the case of the *gapA* operon, this 5′ end represents an overhang of two bases upstream of the stem-loop structure (Fig. 10), whereas in the case of the *ilv-leu* operon, the 5′ end is included in the base pairing of the stem-loop structure (Fig. 7C). The steric shielding of 5′ ends results in mRNA stabilization in *E. coli* as well as in *B. subtilis* (8, 10). In *E. coli*, this can be explained by the fact that the crucial step in the initiation of mRNA degradation, the binding of RNase E, occurs at the 5′ end (28). Efficient attachement of RNase E requires a single-stranded, non-base-paired 5′ end (28). If 5′ ends are protected either by the presence of a stable secondary structure or by the frequent binding of ribosomes to an adjacent Shine-Dalgarno sequence, impaired attachment of RNase E results in increased mRNA stability (8, 10). Although the identity of the RNase E-like enzyme(s) in *B. subtilis* is still unknown, the fact that similar structural determinants at the 5′ end confer mRNA stability in *E. coli* and *B. subtilis* suggests that the mRNA degradation systems might be comparable (10). Most probably, the increased stabilities of the 3′-proximal processing products of the *gapA* and *ilv-leu* operons result from steric exclusion of an enzymatic apparatus which initiates mRNA degradation by binding to 5′ ends.

A further common feature of the processing sites of these operons is the relatively large distance between the 5′ secondary structures and the ribosome-binding sites of the first genes of the generated processing products: the distances between the mapped 5′ ends and the start codons of *gapA* and *ilvC* are 65 and 91 bases, respectively, and the distances between the 5′ stem-loops and the Shine-Dalgarno sequences (AAAGGAGG AAAC and CAAGGGAGAGAT, consensus positions underlined) are 20 and 31 bases. These relatively large leader regions might reflect the necessity of preventing interference of the stem-loop structures with ribosomal subunits: as a 30S ribosomal subunit bound to a Shine-Dalgarno sequence covers a region of around 30 nucleotides (42), too close a neighboring 5′ stabilizing stem-loop could decrease the translation initiation rate by reducing the efficiency of ribosome binding.

The high stability of the monocistronic 1.2-kb *ilvC* processing product caused by the combination of the stem-loop structures at the 5′ and 3′ ends is reflected at the protein level: the amount of IlvC is around 10-fold greater than that of the other proteins encoded by the *ilv-leu* operon. Thus, different amounts of protein are achieved by adjusting the differential stabilities of mRNAs specified by the same operon. There are two further examples of polycistronic *B. subtilis* operons which regulate the amounts of their encoded proteins by differential mRNA stabilities: the *gapA* operon and the *dnaK* operon. For the above-mentioned *gapA* operon, the low stability of the mRNA species which encodes the repressor protein CggR results in a 100-fold-smaller amount of the monomeric form of CggR compared to the product of the second gene of the

operon, *gapA* (31). In this case, the physiological function of this molar ratio is obvious: the gene product of *gapA*, the glyceraldehyde-3-phosphate dehydrogenase, is a metabolic enzyme required in high copy numbers in the cell. In contrast, the repressor protein CggR binds to only a single target sequence located upstream of *cggR* (12) and is consequently required only in very small quantities.

The mRNA species which contain the first gene of the heptacistronic *hrcA-grpE-dnaK-dnaJ-orf35-orf28-orf50* operon also exhibit a very low stability, resulting in a molar ratio of the monomeric forms of the proteins HrcA and DnaK of 1:100 at 37°C and 1:40 at 48°C (21). The physiological function of this molar ratio resembles that postulated for the *gapA* operon: the Hsp70 chaperone of *B. subtilis*, DnaK, is required in large amounts under normal growth conditions and is present in even greater amounts after a temperature upshift. The HrcA protein is the repressor of the class I heat shock operons *hrcA-grpE-dnaK-dnaJ-orf35-orf28-orf50* and *groESL* (41). Because there are only two target sites of this repressor, the required cellular quantities are clearly smaller than those of DnaK. As in the case of the *gapA* operon, an mRNA-processing event generates segments of differential mRNA stability. Cleavage in the intercistronic region between *hrcA* and *grpE* results in a monocistronic upstream *hrcA*-processing product of low stability and a more stable downstream processing product carrying *dnaK*. However, the mapped cleavage site is located within a secondary-structure element and may therefore be recognized by an endoribonuclease different from the one which most probably cleaves the mRNA at the 3′ end of *cggR* and the 5′ end of *ilvC* (21).

For the *ilv-leu* operon, the rationale for the different protein amounts has not yet been identified. On the one hand, the ketol-acid reductoisomerase encoded by *ilvC* may represent a multimeric protein, and the larger amounts of monomeric subunits would result in a comparable molar ratio of the functional enzymes. Indeed, the IlvC proteins of *Salmonella enterica* serovar Typhimurium and *Spinacia oleracea* were shown to form homotetramers (4, 19). However, since the *B. subtilis* IlvC lacks several large stretches of amino acids found in these enzymes, a reliable prediction of a multimeric structure is not possible. *B. subtilis* ketol-acid reductoisomerase may exhibit a low specific activity compared to other enzymes encoded by the *ilv-leu* operon, and the cell compensates for this lower efficiency by having a larger amount of protein. Indeed, the purified *E. coli* enzyme shows a ca. 20-fold-lower specific activity than that of the purified acetolactate synthase encoded by *ilvBH* (7, 18). Although it cannot be assumed that the *B. subtilis* and *E. coli* enzymes have the same properties, the different protein amounts of the branched-chain amino acid biosynthetic enzymes could be explained by different activities of the enzymes encoded by the *ilv-leu* operon.

In summary, the genes for branched-chain amino acid biosynthesis are regulated at different levels. First, the promoters preceding the four trancriptional units involved in this pathway (*ilvA-ypmP*, *ilvBHC-leuABCD*, *ilvD*, and *ybgE*) are under CodY control (33). Second, expression of the *ilv-leu* operon is regulated by tRNA-mediated transcriptional antitermination in response to leucine availability (14, 30). Finally, as demonstrated in the present work, different amounts of the enzymes encoded by the *ilv-leu* operon are adjusted by mRNA processing and differential segmental mRNA stability of the resulting processing products.

ACKNOWLEDGMENTS

We are indebted to Abraham L. Sonenshein for providing strains PS29 and PS37 and to Christian Detsch, Holger Ludwig, Anastasija Matin, Mareike Stieg, and Jörg Stülke for providing strains carrying the translational fusions of *ilvA*, *ilvB*, *ilvD*, and *ybgE* to *lacZ*. We thank Abel Ferrandéz for sharing unbublished results, Claudia Böhnisch for help with the Northern analyses, and Rüdiger Bode for continuous support.

This work was supported by grants from the EU consortium QLG2-CT-1999-01455.

REFERENCES

1. **Aganostopoulos, C., and I. Spizizen.** 1961. Requirements for transformation in *Bacillus subtilis*. J. Bacteriol. **81:**741–746.
2. **Atkinson, M. R., L. V. Wray, Jr., and S. H. Fisher.** 1990. Regulation of histidine and proline degradation enzymes by amino acid availability in *Bacillus subtilis*. J. Bacteriol. **172:**4758–4765.
3. **Belasco, J. G., J. T. Beatty, C. W. Adams, A. von Gabain, and S. N. Cohen.** 1985. Differential expression of photosynthesis genes in *R. capsulata* results from segmental differences in stability within the polycistronic *rxcA* transcript. Cell **40:**171–181.
4. **Biou, V., R. Dumas, C. Cohen-Addad, R. Douce, D. Job, and E. Pebay-Peyroula.** 1997. The crystal structure of plant acetohydroxy acid isomeroreductase complexed with NADPH, two magnesium ions and a herbicidal transition state analog determined at 1.65 A resolution. EMBO J. **16:**3405–3415.
5. **Büttner, K., J. Bernhardt, C. Scharf, R. Schmid, U. Mäder, C. Eymann, H. Antelmann, A. Völker, U. Völker, and M. Hecker.** 2001. A comprehensive two-dimensional map of cytosolic proteins of *Bacillus subtilis*. Electrophoresis **22:**2908–2935.
6. **Chopin, A., V. Biaudet, and S. D. Ehrlich.** 1998. Analysis of the *Bacillus subtilis* genome sequence reveals nine new T-box leaders. Mol. Microbiol. **29:**662–664.
7. **Chunduru, S. K., G. T. Mrachko, and K. C. Calvo.** 1989. Mechanism of ketol acid reductoisomerase — steady-state analysis and metal ion requirement. Biochemistry **28:**486–493.
8. **Coburn, G. A., and G. A. Mackie.** 1999. Degradation of mRNA in *Escherichia coli*: an old problem with some new twists. Prog. Nucleic Acid Res. Mol. Biol. **62:**55–108.
9. **Condon, C., H. Putzer, D. Luo, and M. Grunberg-Manago.** 1997. Processing of the *Bacillus subtilis thrS* leader mRNA is RNase E-dependent in *Escherichia coli*. J. Mol. Biol. **268:**235–242.
10. **Condon, C.** 2003. RNA processing and degradation in *Bacillus subtilis*. Microbiol. Mol. Biol. Rev. **67:**157–174.
11. **De Mendoza, D., G. E. Schujman, and P. S. Aguilar.** 2002. Biosynthesis and function of membrane lipids, p. 405–414. *In* A. L. Sonenshein, J. A. Hoch, and R. Losick (ed.), *Bacillus* and its closest relatives. ASM Press, Washington, D.C.
12. **Doan, T., and S. Aymerich.** 2003. Regulation of the central glycolytic genes in *Bacillus subtilis*: binding of the repressor CggR to its single DNA target sequence is modulated by fructose-1,6-bisphosphate. Mol. Microbiol. **47:**1709–1721.
13. **Eymann, C., G. Homuth, C. Scharf, and M. Hecker.** 2002. *Bacillus subtilis* functional genomics: global characterization of the stringent response by proteome and transcriptome analysis. J. Bacteriol. **184:**2500–2520.
14. **Grandoni, J. A., S. A. Zahler, and J. M. Calvo.** 1992. Transcriptional regulation of the *ilv-leu* operon of *Bacillus subtilis*. J. Bacteriol. **174:**3212–3219.
15. **Grundy, F. J., and T. M. Henkin.** 1994. Conservation of a transcription antitermination mechanism in aminoacyl-tRNA synthetase and amino acid biosynthesis genes in gram-positive bacteria. J. Mol. Biol. **235:**798–804.
16. **Heck, C., R. Rothfuchs, A. Jäger, R. Rauhut, and G. Klug.** 1996. Effect of the *pufQ-pufB* intercistronic region on *puf* mRNA stability in *Rhodobacter capsulatus*. Mol. Microbiol. **20:**1165–1178.
17. **Heck, C., A. Balzer, O. Fuhrmann, and G. Klug.** 2000. Initial events in the degradation of the polycistronic *puf* mRNA in *Rhodobacter capsulatus* and consequences for further processing steps. Mol. Microbiol. **35:**90–100.
18. **Hill, C. H., S. S. Pang, and R. G. Duggleby.** 1997. Purification of *Escherichia coli* acetohydroxyacid synthase isoenzyme II and reconstitution of active enzyme from its individual pure subunits. Biochem. J. **327:**891–898.
19. **Hofler, J. G., C. J. Decedue, G. H. Luginbuhl, J. A. Reynolds, and R. O. Burns.** 1975. The subunit structure of alpha-acetohydroxyacid isomeroreductase from *Salmonella typhimurium*. J. Biol. Chem. **250:**877–882.
20. **Homuth, G., S. Masuda, A. Mogk, Y. Kobayashi, and W. Schumann.** 1997. The *dnaK* operon of *Bacillus subtilis* is heptacistronic. J. Bacteriol. **179:**1153–1164.

21. **Homuth, G., A. Mogk, and W. Schumann.** 1999. Post-transcriptional regulation of the *Bacillus subtilis dnaK* operon. Mol. Microbiol. **32:**1183–1197.
22. **Jäger, S., O. Fuhrmann, C. Heck, M. Hebermehl, E. Schiltz, R. Rauhut, and G. Klug.** 2001. An mRNA degrading complex in *Rhodobacter capsulatus*. Nucleic Acids Res. **29:**4581–4588.
23. **Klug, G., C. W. Adams, J. Belasco, B. Doerge, and S. N. Cohen.** 1987. Biological consequences of segmental alterations in mRNA stability: effects of deletion of the intercistronic hairpin loop region of the *Rhodobacter capsulatus puf* operon. EMBO J. **6:**3515–3520.
24. **Klug, G., and S. N. Cohen.** 1990. Combined actions of multiple hairpin loop structures and sites of rate-limiting endonucleolytic cleavage determine differential degradation rates of individual segments within polycistronic *puf* operon mRNA. J. Bacteriol. **172:**5140–5146.
25. **Kunst, F., N. Ogasawara, I. Moszer, A. M. Albertini, G. Alloni, V. Azevedo, M. G. Bertero, et al.** 1997. The complete genome sequence of the gram-positive bacterium *Bacillus subtilis*. Nature **390:**249–256.
26. **Lopez, J. M., A. Dromerick, and E. Freese.** 1981. Response of guanosine 5′-triphosphate concentration to nutritional changes and its significance for *Bacillus subtilis* sporulation. J. Bacteriol. **146:**605–613.
27. **Ludwig, H., G. Homuth, M. Schmalisch, F. M. Dyka, M. Hecker and J. Stülke.** 2001. Transcription of glycolytic genes and operons in *Bacillus subtilis*: evidence for the presence of multiple levels of control of the *gapA* operon. Mol. Microbiol. **41:**409–422.
28. **Mackie, G. A.** 1998. Ribonuclease E is a 5′-end-dependent endonuclease. Nature **395:**720–723.
29. **Mäder, U., G. Homuth, C. Scharf, K. Büttner, R. Bode, and M. Hecker.** 2002. Transcriptome and proteome analysis of *Bacillus subtilis* gene expression modulated by amino acid availability. J. Bacteriol. **184:**4288–4295.
30. **Marta, P. T., R. D. Ladner, and J. A. Grandoni.** 1996. A CUC triplet confers leucine-dependent regulation of the *Bacillus subtilis ilv-leu* operon. J. Bacteriol. **178:**2150–2153.
31. **Meinken, C., H.-M. Blencke, H. Ludwig, and J. Stülke.** 2003. Expression of the glycolytic *gapA* operon in *Bacillus subtilis*: differential syntheses of proteins encoded by the operon. Microbiology **149:**751–761.
32. **Miller, J.** 1972. Experiments in molecular genetics. Cold Spring Harbor Laboratory Press, Cold Spring Harbor, N.Y.
33. **Molle, V., Y. Nakaura, R. P. Shivers, H. Yamaguchi, R. Losick, Y. Fujita, and A. L. Sonenshein.** 2003. Additional targets of the *Bacillus subtilis* global regulator CodY identified by chromatin immunoprecipitation and genome-wide transcript analysis. J. Bacteriol. **185:**1911–1922.
34. **Pelchat, M., and J. Lapointe.** 1999. Aminoacyl-tRNA synthetase genes of *Bacillus subtilis*: organization and regulation. Biochem. Cell Biol. **77:**343–347.
35. **Ratnayake-Lecamwasam, M., P. Serror, K. W. Wong, and A. L. Sonenshein.** 2001. *Bacillus subtilis* CodY represses early-stationary-phase genes by sensing GTP levels. Genes Dev. **15:**1093–1103.
36. **Schujman, G. E., R. Grau, H. C. Gramajo, L. Ornella, and D. de Mendoza.** 1998. De novo fatty acid synthesis is required for establishment of cell type-specific gene transcription during sporulation in *Bacillus subtilis*. Mol. Microbiol. **29:**1215–1224.
37. **Serror, P., and A. L. Sonenshein.** 1996. CodY is required for nutritional repression of *Bacillus subtilis* genetic competence. J. Bacteriol. **178:**5910–5915.
38. **Stülke, J., R. Hanschke, and M. Hecker.** 1993. Temporal activation of the β-glucanase synthesis in *Bacillus subtilis* is mediated by the GTP pool. J. Gen. Microbiol. **139:**2041–2045.
39. **Versteeg, S., A. Mogk, and W. Schumann.** 1999. The *Bacillus subtilis htpG* gene is not involved in thermal stress management. Mol. Gen. Genet. **261:**582–588.
40. **Wetzstein, M., U. Völker, J. Dedio, S. Löbau, U. Zuber, M. Schiesswohl, C. Herget, M. Hecker, and W. Schumann.** 1992. Cloning, sequencing, and molecular analysis of the *dnaK* locus from *Bacillus subtilis*. J. Bacteriol. **174:**3300–3310.
41. **Yuan, G., and S.-L. Wong.** 1995. Isolation and characterization of *Bacillus subtilis groE* regulatory mutants: evidence for *orf39* in the *dnaK* operon as a repressor gene in regulating the expression of both *groE* and *dnaK*. J. Bacteriol. **177:**6462–6468.
42. **Yusupova, G. Z., M. M. Yusupov, J. H. Cate, and H. F. Noller.** 2001. The path of messenger RNA through the ribosome. Cell **106:**233–241.
43. **Zuker, M.** 2003. Mfold web server for nucleic acid folding and hybridization prediction. Nucleic Acids Res. **31:**3406–3415.